Multiscale Computation for Nano/Micromaterials

James D. Lee[1]; Xianqiao Wang[2]; and Youping Chen[3]

Abstract: This paper presents a multiscale field theory and its applications in modeling and simulation of atomistic systems. The theoretical construction of the multiscale field theory is briefly introduced. A single crystal is discretized into finite-element mesh as if it is a continuous medium. However, each node is a representative unit cell, which contains a specified number of distinctive atoms. Ordinary differential equations for each atom in all nodes are obtained. Material behaviors of a given atomistic system at nano/microscale, subject to the combination of mechanical loadings, electromagnetic field, and temperature field, can be obtained through numerical simulations. Sample problems on wave propagation and simple tension have been solved to demonstrate the advantage and applicability of this multiscale field theory.

DOI: 10.1061/(ASCE)0733-9399(2009)135:3(192)

CE Database subject headings: Computation; Material properties; Simulation.

Introduction

The term "multiscale material modeling" refers to theory and simulation of material properties and behavior across length and time scales from the atomistic to the macroscopic. With the increase in the application of new experimental tools and new material synthesis techniques to nano/microsystems, multiscale material modeling has emerged as a significant approach in computational materials research. Despite widespread interest and efforts, major challenges exist for the simulation of nano/microscale systems over a realistic range of time, length, temperature, as well as in multiple physical conditions and environments. One of the difficulties that arise in such concurrent multiscale modeling is that the high frequency parts of waves are often spuriously reflected at the molecular/continuum interface (Adelman and Doll 1976; Doll and Dion 1976). Actually this is not just a problem at the molecular/continuum interface. In classical finite-element analysis of continuum mechanics, Holmes and Belytschko (1976) were aware of the similar problem in their finite-element models with different element sizes.

In the last decade, many concurrent multiscale techniques have been developed; to begin with, we will briefly review some of these works. The Handshaking method (Abraham et al. 1998; Broughton et al. 1999; Rudd and Broughton 2000; Rudd 2001) is a pioneering work, which incorporates the coupling of a tight-binding quantum mechanics approximation, molecular dynamics (MD), and a finite-element (FE) continuum model. In this method, there is a "handshake" domain where the MD model and the continuum model coexist with averaged Hamiltonian. All of the atoms in the "handshake" domain are in direct correspondence with nodes of the FE mesh. In the continuum region, all of the FEs are modeled as linearly elastic and the elastic moduli are chosen to exactly match those of the underlying atomistic model, thus, minimizing the mismatch across the interface. To reduce spurious wave reflections into the molecular dynamics domain, damping was used in the "handshake" domain, although the damping was not based on any rigorous theory.

In the coarse-grained method formulated by Rudd and Broughton (1998), the fine scale response was modeled in the coarse scale domain by superimposing the atomistic Hamiltonian. The fine scale effects were computed by taking advantage of Bloch symmetry to reduce the size of the dynamic matrix. Their results exhibit excellent phonon spectra and minimal reflection of elastic waves between subdomains, although the results were given only for one-dimensional models.

Cai et al. (2000) introduced a condensation approach to minimize boundary wave reflection. However, it requires the calculation of response functions, which take the form of matrices of size equal to the number of degrees of freedom along the boundary of the MD domain. These matrices are computed by MD simulations on domains somewhat larger than the one of interest.

Wagner and Liu (2003) have developed a bridging-scale method in which the molecular displacements are decomposed into fine and coarse scales throughout the domain. However, in the coarse scale domain, the fine scale features are not modeled explicitly. At the interface between the two domains, they use a form of the Langevin equation to eliminate spurious reflections. They reported excellent results for one-dimensional problems. Karpov et al. (2005) have developed coupling methods based on lattice dynamics. In this method, the spurious reflections at the edge of the molecular model are eliminated by introducing forces equivalent to the lattice impedance; this entails the evaluation of inverse Laplace transforms in time, and for multidimensional problems, a Fourier transform in space. The method is very effective for linear continua, but the extension to nonlinear response may be difficult. To and Li (2005) proposed to combine the bridging-scale method with the perfectly matched-layer method to

[1]Professor, Dept. of Mechanical and Aerospace Engineering, George Washington Univ., Washington, DC 20052. E-mail: jdlee@gwu.edu

[2]Research Assistant, Dept. of Mechanical and Aerospace Engineering, George Washington Univ., Washington, DC 20052. E-mail: xqwang@gwu.edu

[3]Assistant Professor, Dept. of Mechanical and Aerospace Engineering, Univ. of Florida, Gainesville, FL 32611. E-mail: ypchen2@ufl.edu

Note. Associate Editor: George Z. Voyiadjis. Discussion open until August 1, 2009. Separate discussions must be submitted for individual papers. The manuscript for this paper was submitted for review and possible publication on September 11, 2007; approved on September 26, 2008. This paper is part of the ***Journal of Engineering Mechanics***, Vol. 135, No. 3, March 1, 2009. ©ASCE, ISSN 0733-9399/2009/3-192–202/$25.00.

eliminate the spurious reflections by matching the impedance at the atomistic/continuum interface.

A heterogeneous multiscale method has been developed by E and his co-workers (E and Huang 2001, 2002; Li and E 2005). It is based on the concept that both the atomistic and the continuum models are formulated in the form of conservation laws of mass, momentum, and energy. The strategy is to start with a macroscale solver and find the missing macroscale data such as the constitutive laws and kinetic relation by performing local simulations of the microscale models constrained to be consistent with a local macroscale state of the system. More details can be found in a review article (E et al. 2007).

In the bridging-domain method, the continuum and molecular domains are overlapped in a bridging subdomain, where the Hamiltonian is taken to be a linear combination of the continuum and molecular Hamiltonian (Belytschko and Xiao 2003; Xiao and Belytschko 2004). The compatibility in the bridging domain is enforced by Lagrange multipliers or by the augmented Lagrangian method. This method is aimed at crystalline or amorphous solids, and it is assumed that the deformations are sufficiently small and so that voids or dislocations do not develop in the continuum subdomain. Results show that this method can avoid spurious wave reflections at the molecular/continuum interface without any additional filtering procedures. A multiple-time-step algorithm is also developed within this framework.

Generally speaking, in all those above-mentioned coupled methods, the idea is to use a fully atomistic description in one region of material and a continuum description in other regions. The detailed treatment of the material in the "transition region" or boundary between the atomistic and continuum regions is a critical aspect of such an approach. Nearly all of the existing methods have a well-defined transition region in which some approximation is made. An approximation is necessary due to the fundamental incompatibility of the nonlocal atomistic description and the local continuum description. Variations among the existing coupling methods are a result of differences in desired application of the method, intuitive identification of important physical phenomena, and issues related to practical, computationally efficient implementation. Curtin and Miller (2003) gave a review of these methods and noted that a unified and formal theory of the transition region that allows quantifiable error bounds to be established does not yet exist.

The quasicontinuum (QC) method (Tadmor et al. 1996) has been used to study a variety of fundamental aspects of deformation in crystalline solids. The QC method defines two types of atoms, "local representative atoms" and "nonlocal representative atoms," rather than identifying atomistic and continuum regions. In practice, however, the regions containing nonlocal representative atoms are essentially equivalent to the fully atomistic regions of other methods. Similarly, a local representative atom is coincident with either a continuum FE node or an atomic position near a Gauss point used to define the energy of the continuum element. The language of nonlocal and local clearly associates the nonlocal atoms with "real" atoms and the local atoms with the local FE region. The interface atoms are included in the atomistic energy but are also FE nodes of the continuum. The pad atom positions are dictated by interpolation from the FE nodal positions. The pad atom energies are not included, but the energies of the real and interface atoms include their interactions with the pad atoms. To avoid overcounting of the energy of the interface atoms/nodes, the energies of the continuum elements adjacent to the interface (i.e., elements that have nodes corresponding to the interface atoms as shown in gray in the figure) are weighted differently in the total potential energy sum. The total potential energy of the QC model is then obtained by summing the energies of all atoms in the atomistic region and at the interface and all elements in the continuum domain. The QC potential energy leads to some nonphysical effects in the transition region, as alluded to in the previous section. Specifically, taking derivatives of the energy functional to obtain forces on atoms and finite-element (FE) nodes leads to so-called ghost forces in the transition region (Shenoy et al. 1998). The origin of these ghost forces lies precisely in the assumption of locality in the continuum region and the local/nonlocal mismatch in the transition region. Later, Knap and Ortiz (2001) have proposed a QC formulation that is entirely "nonlocal" in that the locality implicit in an FE calculation is eliminated. The overall concept is to use FE ideas to kinematically constrain some atomic positions to node positions but to determine forces from a fully nonlocal atomistic description at all times and in all regions of space. The Cauchy-Born rule is, thus, abandoned and forces are calculated from clusters of representative atoms centered on atoms corresponding to FE nodes. An order-N atomic-scale finite-element method, called AFEM, was proposed by Liu et al. (2004). It is as accurate as MD simulations, but much faster than the order-N^2 conjugate gradient method. Hence, it is suitable for large-scale static problems. Recently, Dupuy et al. (2005), using a combination of statistical mechanics and finite-element interpolation, developed a coarse-grained alternative to molecular dynamics for crystalline solids at a constant temperature.

In a series of theoretical papers, a multiscale field theory has been constructed by Chen and her co-workers (Chen 2006; Chen and Lee 2005, 2006; Chen et al. 2006a, b; Xiong et al. 2007) for concurrent atomic-continuum modeling of materials/systems. Continuous local densities of fundamental physical quantities in atomistic systems are derived. By decomposing atomic motion/deformation into homogeneous lattice motion/deformation and inhomogeneous internal atomic motion/deformation, and also decomposing momentum flux and heat flux into homogeneous and inhomogeneous parts, field description of conservation laws at atomic scale has been formulated. As a result of the formulation, a field representation of atomic many-body dynamics is obtained, and time-interval averaged quantities can be solved. Since the conservation equations obtained by Chen (2006), Chen and Lee (2006), and Chen et al. (2006a) are valid at atomic scale, the field theory can reproduce time averaged atomic trajectories and can be used to investigate phenomena and properties that originated at atomic scale. Since it is a field theory formulated in terms of time interval averaged quantities, it is expected to be computationally more efficient than atomic-level MD simulation, and can be applied to simulate phenomena at larger length and time scales.

The outline of this paper is as follows: in the section of Multiscale Field Theory, we briefly introduce our multiscale theory, including the derivations of the balance law of linear momentum and constitutive equations for momentum flux. Although the theory is based on atomic many-body dynamics, we end up with a continuum field theory. Therefore, in the next section, we do a Finite-Element Formulation for this multiscale theory. In the section of Sample Problems, we present the numerical results of two sets of sample problems to demonstrate the characteristics and the advantages of the theory and its numerical algorithm. In the last section, we give a Summary and Discussion, including the comparisons with other multiscale theories.

Multiscale Field Theory

Crystalline solids are distinguished from other states of matter by a periodic arrangement of the atoms; such a structure is called a crystal lattice. Essentially the regularity displayed by a crystal lattice is that of a three-dimensional mesh, which divides space into identical parallelepipeds. Imagine a number of identical atoms placed at the intersections of such a mesh; then we have what is known as a simple lattice (or Bravais lattice).

Microscopic dynamic quantities are functions of phase-space coordinates $(\mathbf{r},\mathbf{p})$, i.e., the positions and momenta of atoms. For multielement systems, there is more than one atom in the unit cell. Thus, one has

$$\mathbf{r} = \{\mathbf{R}^{k\alpha} = \mathbf{R}^k + \Delta\mathbf{r}^{k\alpha} | k = 1,2,3,\ldots n,\ \ \alpha = 1,2,3,\ldots \nu\}$$

$$\mathbf{p} = \{m^\alpha \mathbf{V}^{k\alpha} = m^\alpha \mathbf{V}^k + m^\alpha \Delta\mathbf{v}^{k\alpha} | k = 1,2,3\ldots n,\ \ \alpha = 1,2,3,\ldots \nu\} \tag{1}$$

where the superscript $k\alpha$ refers to the αth atom in the kth unit cell; m^α=mass of the αth atom; $\mathbf{R}^{k\alpha}$ and $\mathbf{V}^{k\alpha}$=position and velocity vector of the $k\alpha$ atom, respectively; $\mathbf{R}^k$ and $\mathbf{V}^k$=position and velocity of the mass center of the kth unit cell, respectively; $\Delta\mathbf{r}^{k\alpha}$ and $\Delta\mathbf{v}^{k\alpha}$=atomic position and velocity of the αth atom relative to the mass center of the kth unit cell, respectively; n=total number of unit cells in the system; υ=number of atoms in a unit cell. The local density of any measurable phase-space function $\mathbf{a}(\mathbf{r},\mathbf{p})$ can generally be defined as

$$\mathbf{A}(\mathbf{x},\mathbf{y}^\alpha,t) = \sum_{k=1}^{n}\sum_{\xi=1}^{\nu} \mathbf{a}\{\mathbf{r}(t),\mathbf{p}(t)\}\delta(\mathbf{R}^k - \mathbf{x})\tilde{\delta}(\Delta\mathbf{r}^{k\xi} - \mathbf{y}^\alpha) \equiv \mathbf{A}^\alpha(\mathbf{x},t) \tag{2}$$

The first delta function in Eq. (2) is a localization function that provides the link between phase space and physical space descriptions. It can be a Dirac δ-function (Irvine and Kirkwood 1950) or a distribution function (Hardy 1982), such as

$$\delta(\mathbf{R}^k - \mathbf{x}) = \pi^{-3/2} l^{-3} e^{-|\mathbf{R}^k - \mathbf{x}|/l^2} \tag{3}$$

The field descriptions of the conservation equations and the constitutive relations (the interrelations between field quantities) are found to be independent of the choices of the localization function (Hardy 1982; Chen and Lee 2005, 2006; Chen et al. 2006a). The second delta function in Eq. (2) is the Kronecker delta, which identifies $\mathbf{y}^\alpha$ to $\Delta\mathbf{r}^{k\alpha}$. It can be easily proved that the following normalization condition holds

$$\int_{\Omega(\mathbf{x})} \delta(\mathbf{R}^k - \mathbf{x})\tilde{\delta}(\Delta\mathbf{r}^{k\alpha} - \mathbf{y}^\alpha) d^3\Omega(\mathbf{x}) = 1$$
$$(k = 1,2,3,\ldots n)\ \ (\alpha = 1,2,\ldots \nu) \tag{4}$$

It is also obvious that the distribution function satisfies the following identity as the Dirac delta function does

$$\frac{\partial\delta(\mathbf{R}^{k\alpha} - \mathbf{x})}{\partial\mathbf{R}^{k\alpha}} = -\frac{\partial\delta(\mathbf{R}^{k\alpha} - \mathbf{x})}{\partial\mathbf{x}} \tag{5}$$

Most current MD applications involve systems that are either in equilibrium or in some time-independent stationary state, where individual results are subjected to fluctuation; it is the well-defined averages over sufficiently long time intervals that are of interest. To smooth out the results and to obtain results close to experiments, measurements of physical quantities are necessary to be collected and averaged over a finite-time duration. Therefore, in deriving the field description of atomic quantities and balance equations, it is the time-interval averaged quantities that are used, and the time-interval averaged (at time t in the interval $[t,\ t+\Delta t]$) local density function takes the form

$$\bar{A}^\alpha(\mathbf{x},t) = \langle A^\alpha\rangle \equiv \frac{1}{\Delta t}\int_0^{\Delta t} A^\alpha(\mathbf{x},t+\tau)d\tau$$
$$= \frac{1}{\Delta t}\int_0^{\Delta t}\sum_{k=1}^{n} a(\mathbf{r}(t+\tau),\mathbf{p}(t+\tau))$$
$$\times\delta(\mathbf{R}^k - \mathbf{x})\tilde{\delta}(\Delta\mathbf{r}^{k\alpha} - \mathbf{y}^\alpha)d\tau \tag{6}$$

The mathematical representation of conservation equations for mass, linear momentum, and energy at atomic scale has been analytically obtained in terms of averaged field quantities (Chen and Lee 2005, 2006; Chen et al. 2006a). In this work, we are only concerned with "one-way coupling" with temperature and electromagnetic fields, i.e., the temperature and electromagnetic fields are given as functions of space and time. The relevant governing equations are then just the balance laws for linear momentum

$$\frac{\partial}{\partial t}[\bar{\rho}^\alpha(\bar{\mathbf{v}} + \Delta\bar{\mathbf{v}}^\alpha)] = \nabla_{\mathbf{x}}\cdot[\bar{\mathbf{t}}^\alpha - \bar{\rho}^\alpha\bar{\mathbf{v}}\otimes(\bar{\mathbf{v}} + \Delta\bar{\mathbf{v}}^\alpha)]$$
$$+ \nabla_{\mathbf{y}^\alpha}\cdot[\bar{\boldsymbol{\tau}}^\alpha - \bar{\rho}^\alpha\Delta\bar{\mathbf{v}}^\alpha\otimes(\bar{\mathbf{v}} + \Delta\bar{\mathbf{v}}^\alpha)] + \bar{\boldsymbol{\varphi}}^\alpha \tag{7}$$

where the time interval averaged mass density $\bar{\rho}^\alpha$, linear momentum $\bar{\rho}^\alpha(\bar{\mathbf{v}}+\Delta\bar{\mathbf{v}}^\alpha)$, homogeneous atomic stresses $\bar{\mathbf{t}}^\alpha_{(\mathrm{kin})}+\bar{\mathbf{t}}^\alpha_{(\mathrm{pot})}$ and inhomogeneous atomic stresses $\bar{\boldsymbol{\tau}}^\alpha_{(\mathrm{kin})}+\bar{\boldsymbol{\tau}}^\alpha_{(\mathrm{pot})}$, and body force density $\bar{\boldsymbol{\varphi}}^\alpha$ are defined as

$$\bar{\rho}^\alpha(\mathbf{x},t) \equiv \left\langle \sum_{k=1}^{n} m^\alpha\delta(\mathbf{R}^k - \mathbf{x})\tilde{\delta}(\Delta\mathbf{r}^{k\alpha} - \mathbf{y}^\alpha)\right\rangle \tag{8}$$

$$\bar{\rho}^\alpha(\bar{\mathbf{v}} + \Delta\bar{\mathbf{v}}^\alpha) \equiv \left\langle \sum_{k=1}^{n} m^\alpha(\mathbf{V}^k + \Delta\mathbf{v}^{k\alpha})\delta(\mathbf{R}^k - \mathbf{x})\tilde{\delta}(\Delta\mathbf{r}^{k\alpha} - \mathbf{y}^\alpha)\right\rangle \tag{9}$$

$$\bar{\mathbf{t}}^\alpha_{(\mathrm{kin})} \equiv -\left\langle \sum_{k=1}^{n} m^\alpha\tilde{\mathbf{V}}^k\otimes\tilde{\mathbf{V}}^{k\alpha}\delta(\mathbf{R}^k - \mathbf{x})\tilde{\delta}(\Delta\mathbf{r}^{k\alpha} - \mathbf{y}^\alpha)\right\rangle \tag{10}$$

$$\bar{\boldsymbol{\tau}}^\alpha_{(\mathrm{kin})} \equiv -\left\langle \sum_{k=1}^{n} m^\alpha\Delta\tilde{\mathbf{v}}^{k\alpha}\otimes\tilde{\mathbf{V}}^{k\alpha}\delta(\mathbf{R}^k - \mathbf{x})\tilde{\delta}(\Delta\mathbf{r}^{k\alpha} - \mathbf{y}^\alpha)\right\rangle \tag{11}$$

$$\bar{\mathbf{t}}^\alpha_{(\mathrm{pot})} \equiv -\frac{1}{2}\left\langle \sum_{k,l=1}^{n}\sum_{\xi,\eta=1}^{\nu} (\mathbf{R}^k - \mathbf{R}^l)\otimes\mathbf{F}^{k\xi}B(k,\xi,l,\eta,\mathbf{x},\mathbf{y}^\alpha)\right\rangle \tag{12}$$

$$\bar{\boldsymbol{\tau}}^\alpha_{(\mathrm{pot})} \equiv -\frac{1}{2}\left\langle \sum_{k,l=1}^{n}\sum_{\xi,\eta=1}^{\nu} (\Delta\mathbf{r}^{k\xi} - \Delta\mathbf{r}^{l\eta})\otimes\mathbf{F}^{k\xi}B(k,\xi,l,\eta,\mathbf{x},\mathbf{y}^\alpha)\right\rangle \tag{13}$$

$$\bar{\boldsymbol{\varphi}}^\alpha \equiv \left\langle \sum_{k=1}^{n} \boldsymbol{\varphi}^{k\alpha}\delta(\mathbf{R}^k - \mathbf{x})\tilde{\delta}(\Delta\mathbf{r}^{k\alpha} - \mathbf{y}^\alpha)\right\rangle \tag{14}$$

where $\mathbf{F}^{k\xi}$=interatomic force acting on the $k\xi$ atom; $\boldsymbol{\varphi}^{k\alpha}$=body force acting on the $k\alpha$ atom

$$\tilde{\mathbf{V}}^{k\alpha} \equiv \mathbf{V}^{k\alpha} - \bar{\mathbf{v}} - \Delta\bar{\mathbf{v}}^{\alpha} \quad \tilde{\mathbf{V}}^{k} \equiv \mathbf{V}^{k} - \bar{\mathbf{v}} \quad \Delta\tilde{\mathbf{v}}^{k\alpha} \equiv \Delta\mathbf{v}^{k\alpha} - \Delta\bar{\mathbf{v}}^{\alpha} \tag{15}$$

$$B(k,\xi,l,\eta,\mathbf{x},\mathbf{y}^{\alpha}) \equiv \int_0^1 \delta(\mathbf{R}^k\lambda + \mathbf{R}^l(1-\lambda) - \mathbf{x}) \times \tilde{\delta}(\Delta\mathbf{r}^{k\xi}\lambda + \Delta\mathbf{r}^{l\eta}(1-\lambda) - \mathbf{y}^{\alpha})d\lambda \tag{16}$$

It is worthwhile to note that, with the atomistic definitions of interatomic force and the potential parts of the atomic stresses, one has

$$\nabla_{\mathbf{x}} \cdot \bar{\mathbf{t}}^{\alpha}_{\text{pot}} + \nabla_{\mathbf{y}^{\alpha}} \cdot \bar{\boldsymbol{\tau}}^{\alpha}_{\text{pot}} = \bar{\mathbf{f}}^{\alpha} \tag{17}$$

where $\bar{\mathbf{f}}^{\alpha}$=interatomic force density acting on the αth atom in the unit cell located at $\mathbf{x}$.

Finite-Element Formulation

From now on, we work with time interval averaged quantities. For simplicity, we drop the bars on top of the quantities if it does not cause ambiguity. The governing equations [Eq. (7)] can now be rewritten as

$$\rho^{\alpha}\ddot{\mathbf{u}}^{\alpha} = \nabla_{\mathbf{x}} \cdot \mathbf{t}^{\alpha} + \nabla_{\mathbf{y}^{\alpha}} \cdot \boldsymbol{\tau}^{\alpha} + \mathbf{f}^{\alpha}/V^* + \boldsymbol{\varphi}^{\alpha}/V^* \tag{18}$$

where $\mathbf{u}^{\alpha}$=displacement vector of the αth atom; V^*=volume of unit cell; and from now on, $\mathbf{t}^{\alpha}$ and $\boldsymbol{\tau}^{\alpha}$=kinetic part of the homogeneous and inhomogeneous atomic stresses associated with the αth atom, respectively. For a single-element atomic system, Cheung and Yip (1991) and Haile (1992) gave the following definitions for kinetic stresses $\hat{t}_{ij}$ and temperature $\hat{T}$:

$$\hat{t}_{ij} = -\left\langle \sum_{l=1}^{N} m\tilde{v}_i^l\tilde{v}_j^l \right\rangle \Big/ \hat{V} \tag{19}$$

$$3Nk_B\hat{T} = \left\langle \sum_{l=1}^{N} m\tilde{v}_i^l\tilde{v}_i^l \right\rangle \tag{20}$$

where k_B=Boltzmann constant; and $\hat{V}$=volume that the N atoms occupy. Consistent with Cheung and Yip (1991) and Haile (1992), for a multielement atomic system, we have

$$\mathbf{t}^{\alpha}_{ij} = -\langle m^{\alpha}\tilde{v}_i(\tilde{v}_j + \Delta\tilde{v}_j^{\alpha})\rangle/V^* \quad \tau^{\alpha}_{ij} = -\langle m^{\alpha}\Delta\tilde{v}_i^{\alpha}(\tilde{v}_j + \Delta\tilde{v}_j^{\alpha})\rangle/V^* \tag{21}$$

$$3k_BT^{\alpha} = \langle m^{\alpha}(\tilde{v}_i + \Delta\tilde{v}_i^{\alpha})(\tilde{v}_i + \Delta\tilde{v}_i^{\alpha})\rangle \tag{22}$$

At temperature higher than Debye temperature and within harmonic approximation, all modes have the same energy (Dove 1993). This implies

$$(\upsilon - 1)\langle M\tilde{v}_i\tilde{v}_i\rangle = \left\langle \sum_{\alpha=1}^{\upsilon} m^{\alpha}\Delta\tilde{v}_i^{\alpha}\Delta\tilde{v}_i^{\alpha} \right\rangle \tag{23}$$

where $M \equiv \sum_{\alpha=1}^{\upsilon} m^{\alpha}$=total mass of a unit cell. Definition of temperature at nanoscale is still a debated issue. Here, we follow the classical way to define temperature as a measure of thermal energy over a finite-duration and over a unit cell. Thus, we have $T^{\alpha}=T(\mathbf{x},t)$ and $\nabla_{\mathbf{y}^{\alpha}}\cdot\boldsymbol{\tau}^{\alpha}=0$. Now the governing equation [Eq. (18)] can be rewritten as

$$m^{\alpha}\ddot{\mathbf{u}}^{\alpha} = V^*\nabla \cdot \mathbf{t}^{\alpha} + \mathbf{f}^{\alpha} + \boldsymbol{\varphi}^{\alpha} \tag{24}$$

with

$$t^{\alpha}_{ij} = -\gamma^{\alpha}k_BT\delta_{ij}/V^* \quad \tau^{\alpha}_{ij} = -(1-\gamma^{\alpha})k_BT\delta_{ij}/V^* \quad \gamma^{\alpha} \equiv m^{\alpha}/M$$

In this work, we study the cases of which the temperature field is constant in space, including $T=0$ as a special case. To demonstrate the derivation of the finite-element formulation in detail, we write the interatomic force as

$$\mathbf{f}^{\alpha}(\mathbf{x}) = \int_{\Omega(\mathbf{x}')} \sum_{\beta=1}^{\upsilon} \mathbf{f}^{\alpha\beta}[\mathbf{u}^{\alpha}(\mathbf{x}),\mathbf{u}^{\beta}(\mathbf{x}')]\frac{d\Omega(\mathbf{x}')}{V^*(\mathbf{x}')} \tag{25}$$

where $\mathbf{f}^{\alpha\beta}[\mathbf{u}^{\alpha}(\mathbf{x}),\mathbf{u}^{\beta}(\mathbf{x}')]$=force acting on the αth atom in the unit cell embedded at $\mathbf{x}$ due to the interaction with the βth atom in the unit cell embedded at $\mathbf{x}'$. The interatomic force $\mathbf{f}^{\alpha\beta}$ is parallel to $\mathbf{r}^{\alpha\beta}(\mathbf{x},\mathbf{x}') \equiv \mathbf{x}+\Delta\mathbf{x}^{\alpha}+\mathbf{u}^{\alpha}(\mathbf{x})-[\mathbf{x}'+\Delta\mathbf{x}'^{\beta}+\mathbf{u}^{\beta}(\mathbf{x}')]$ and the magnitude is a function of the distance between atom α and atom β, i.e., $r^{\alpha\beta}=\|\mathbf{r}^{\alpha\beta}\|$. The function form and the integral emphasize the nonlinear and nonlocal characteristics of the interatomic forces. Now the weak form of Eq. (24), with $T=0$, can be obtained by the Galerkin method as

$$\sum_{\alpha=1}^{\upsilon}\int_{\Omega(\mathbf{x})}\left(m^{\alpha}\ddot{\mathbf{u}}^{\alpha}(\mathbf{x}) - \int_{\Omega(\mathbf{x}')}\sum_{\beta=1}^{\upsilon}\mathbf{f}^{\alpha\beta}[\mathbf{u}^{\alpha}(\mathbf{x}),\mathbf{u}^{\beta}(\mathbf{x}')] \times\frac{d\Omega(\mathbf{x}')}{V^*(\mathbf{x}')} - \boldsymbol{\varphi}^{\alpha}\right)\cdot\delta\mathbf{u}^{\alpha}(\mathbf{x})\frac{d\Omega(\mathbf{x})}{V^*(\mathbf{x})} = 0 \tag{26}$$

where $\delta\mathbf{u}^{\alpha}(\mathbf{x})$=virtual displacement of the αth atom in the unit cell embedded at $\mathbf{x}$. Suppose the finite-element mesh of the specimen has N_p nodes, N_e eight-node 3D brick-type elements, each with eight Gauss points and the displacement field can be approximated as

$$\mathbf{u}^{\alpha}(\mathbf{x}) = \Phi_{\xi}(\mathbf{x})\mathbf{U}^{\xi\alpha} \quad \delta\mathbf{u}^{\alpha}(\mathbf{x}) = \Phi_{\xi}(\mathbf{x})\delta\mathbf{U}^{\xi\alpha} \tag{27}$$

where $\mathbf{U}^{\xi\alpha}$ and $\delta\mathbf{U}^{\xi\alpha}$=corresponding nodal values of $\mathbf{u}^{\alpha}(\mathbf{x})$ and $\delta\mathbf{u}^{\alpha}(\mathbf{x})$; $\Phi_{\xi}(\mathbf{x})$=shape functions; the summation over ξ is understood. Eq. (26) can then be rewritten as

$$\sum_{\alpha=1}^{\upsilon}\int_{\Omega(\mathbf{x})} m^{\alpha}\boldsymbol{\Phi}_{\eta}(\mathbf{x})\boldsymbol{\Phi}_{\xi}(\mathbf{x})\ddot{\mathbf{U}}^{\xi\alpha}\cdot\delta\mathbf{U}^{\eta\alpha}\frac{d\Omega(\mathbf{x})}{V^*(\mathbf{x})} - \sum_{\alpha=1}^{\upsilon}\sum_{\beta=1}^{\upsilon}\int_{\Omega(\mathbf{x})}\int_{\Omega(\mathbf{x}')}\boldsymbol{\Phi}_{\eta}(\mathbf{x})\mathbf{f}^{\alpha\beta}[\mathbf{u}^{\alpha}(\mathbf{x}),\mathbf{u}^{\beta}(\mathbf{x}')]\cdot\delta\mathbf{U}^{\eta\alpha} \times\frac{d\Omega(\mathbf{x}')}{V^*(\mathbf{x}')}\frac{d\Omega(\mathbf{x})}{V^*(\mathbf{x})} - \sum_{\alpha=1}^{\upsilon}\int_{\Omega(\mathbf{x})}\boldsymbol{\Phi}_{\eta}(\mathbf{x})\boldsymbol{\varphi}^{\alpha}\cdot\delta\mathbf{U}^{\eta\alpha}\frac{d\Omega(\mathbf{x})}{V^*(\mathbf{x})} = 0 \tag{28}$$

Since

$$\sum_{\alpha=1}^{\upsilon}\sum_{\beta=1}^{\upsilon}\int_{\Omega(\mathbf{x})}\int_{\Omega(\mathbf{x}')}\mathbf{\Phi}_{\eta}(\mathbf{x})\mathbf{f}^{\alpha\beta}[\mathbf{u}^{\alpha}(\mathbf{x}),\mathbf{u}^{\beta}(\mathbf{x}')]\cdot\delta\mathbf{U}^{\eta\alpha}\frac{d\Omega(\mathbf{x})}{V^{*}(\mathbf{x})}\frac{d\Omega(\mathbf{x}')}{V^{*}(\mathbf{x}')}$$
$$=\sum_{\alpha=1}^{\upsilon}\sum_{\beta=1}^{\upsilon}\int_{\Omega(\mathbf{x})}\int_{\Omega(\mathbf{x}')}\mathbf{\Phi}_{\eta}(\mathbf{x}')\mathbf{f}^{\beta\alpha}[\mathbf{u}^{\beta}(\mathbf{x}'),\mathbf{u}^{\alpha}(\mathbf{x})]\cdot\delta\mathbf{U}^{\eta\beta}\times\frac{d\Omega(\mathbf{x})}{V^{*}(\mathbf{x})}\frac{d\Omega(\mathbf{x}')}{V^{*}(\mathbf{x}')}$$

and

$$\mathbf{f}^{\alpha\beta}[\mathbf{u}^{\alpha}(\mathbf{x}),\mathbf{u}^{\beta}(\mathbf{x}')]=-\mathbf{f}^{\beta\alpha}[\mathbf{u}^{\beta}(\mathbf{x}'),\mathbf{u}^{\alpha}(\mathbf{x})]$$

Eq. (28) can be rewritten as

$$\sum_{\alpha=1}^{\upsilon}\int_{\Omega(\mathbf{x})}m^{\alpha}\mathbf{\Phi}_{\eta}(\mathbf{x})\mathbf{\Phi}_{\xi}(\mathbf{x})\ddot{\mathbf{U}}^{\xi\alpha}\cdot\delta\mathbf{U}^{\eta\alpha}\frac{d\Omega(\mathbf{x})}{V^{*}(\mathbf{x})}$$
$$-\frac{1}{2}\sum_{\alpha=1}^{\upsilon}\sum_{\beta=1}^{\upsilon}\int_{\Omega(\mathbf{x})}\int_{\Omega(\mathbf{x}')}\mathbf{\Phi}_{\eta}(\mathbf{x})\mathbf{f}^{\alpha\beta}[\mathbf{u}^{\alpha}(\mathbf{x}),\mathbf{u}^{\beta}(\mathbf{x}')]\cdot\delta\mathbf{U}^{\eta\alpha}\times\frac{d\Omega(\mathbf{x})}{V^{*}(\mathbf{x})}\frac{d\Omega(\mathbf{x}')}{V^{*}(\mathbf{x}')}$$
$$+\frac{1}{2}\sum_{\alpha=1}^{\upsilon}\sum_{\beta=1}^{\upsilon}\int_{\Omega(\mathbf{x})}\int_{\Omega(\mathbf{x}')}\mathbf{\Phi}_{\eta}(\mathbf{x}')\mathbf{f}^{\alpha\beta}[\mathbf{u}^{\alpha}(\mathbf{x}),\mathbf{u}^{\beta}(\mathbf{x}')]\cdot\delta\mathbf{U}^{\eta\beta}\times\frac{d\Omega(\mathbf{x})}{V^{*}(\mathbf{x})}\frac{d\Omega(\mathbf{x}')}{V^{*}(\mathbf{x}')}-\sum_{\alpha=1}^{\upsilon}\int_{\Omega(\mathbf{x}')}\mathbf{\Phi}_{\eta}(\mathbf{x})\boldsymbol{\varphi}^{\alpha}\cdot\delta\mathbf{U}^{\eta\alpha}\frac{d\Omega(\mathbf{x})}{V^{*}(\mathbf{x})}=0 \quad (29)$$

The derivation from Eqs. (28) and (29) is to ensure that the summation of interatomic force is vanishing. In this work, we are using full order integration. Denote also

$$I(\xi)\equiv IJK(I_e,\xi)\quad J(\eta)\equiv IJK(\mathbf{x}',\eta) \quad (30)$$

where IJK stands for the connectivity of the finite-element mesh; in other words, $I(\xi)$=node number of the ξth node of the I_eth element; and $J(\eta)$=node number of the ηth node of the element in which $\mathbf{x}'$ is located. Now, each term in Eq. (29) can be further derived to be

$$\sum_{\alpha=1}^{\upsilon}\int_{\Omega(\mathbf{x})}m^{\alpha}\mathbf{\Phi}_{\eta}(\mathbf{x})\mathbf{\Phi}_{\xi}(\mathbf{x})\ddot{\mathbf{U}}^{\xi\alpha}\cdot\delta\mathbf{U}^{\eta\alpha}\frac{d\Omega(\mathbf{x})}{V^{*}(\mathbf{x})}$$
$$\approx\sum_{\alpha=1}^{\upsilon}\sum_{I_e=1}^{N_e}\sum_{g=1}^{8}m^{\alpha}\mathbf{\Phi}_{\eta}(I_e,g)\mathbf{\Phi}_{\xi}(I_e,g)\frac{J(I_e,g)}{V^{*}(I_e,g)}\ddot{\mathbf{U}}^{I(\xi),\alpha}\cdot\delta\mathbf{U}^{I(\eta),\alpha} \quad (31)$$

$$-\frac{1}{2}\sum_{\alpha=1}^{\upsilon}\sum_{\beta=1}^{\upsilon}\int_{\Omega(\mathbf{x})}\int_{\Omega(\mathbf{x}')}\mathbf{\Phi}_{\eta}(\mathbf{x})\mathbf{f}^{\alpha\beta}[\mathbf{u}^{\alpha}(\mathbf{x}),\mathbf{u}^{\beta}(\mathbf{x}')]\cdot\delta\mathbf{U}^{\eta\alpha}\frac{d\Omega(\mathbf{x})}{V^{*}(\mathbf{x})}\frac{d\Omega(\mathbf{x}')}{V^{*}(\mathbf{x}')}$$
$$\approx-\frac{1}{2}\sum_{\alpha=1}^{\upsilon}\sum_{\beta=1}^{\upsilon}\sum_{I_e=1}^{N_e}\sum_{g=1}^{8}\mathbf{\Phi}_{\eta}(I_e,g)\frac{J(I_e,g)}{V^{*}(I_e,g)}\left\{\int_{\Omega(\mathbf{x}')}\mathbf{f}^{\alpha\beta}[\mathbf{u}^{\alpha}(I_e,g),\mathbf{u}^{\beta}(\mathbf{x}')]\frac{d\Omega(\mathbf{x}')}{V^{*}(\mathbf{x}')}\right\}\cdot\delta\mathbf{U}^{I(\eta),\alpha} \quad (32)$$

$$\frac{1}{2}\sum_{\alpha=1}^{\upsilon}\sum_{\beta=1}^{\upsilon}\int_{\Omega(\mathbf{x})}\int_{\Omega(\mathbf{x}')}\mathbf{\Phi}_{\eta}(\mathbf{x}')\mathbf{f}^{\alpha\beta}[\mathbf{u}^{\alpha}(\mathbf{x}),\mathbf{u}^{\beta}(\mathbf{x}')]\cdot\delta\mathbf{U}^{\eta\beta}\frac{d\Omega(\mathbf{x})}{V^{*}(\mathbf{x})}\frac{d\Omega(\mathbf{x}')}{V^{*}(\mathbf{x}')}$$
$$\approx\frac{1}{2}\sum_{\alpha=1}^{\upsilon}\sum_{\beta=1}^{\upsilon}\sum_{I_e=1}^{N_e}\sum_{g=1}^{8}\frac{J(I_e,g)}{V^{*}(I_e,g)}\left\{\int_{\Omega(\mathbf{x}')}\mathbf{\Phi}_{\eta}(\mathbf{x}')\mathbf{f}^{\alpha\beta}[\mathbf{u}^{\alpha}(I_e,g),\mathbf{u}^{\beta}(\mathbf{x}')]\cdot\delta\mathbf{U}^{J(\eta),\beta}\frac{d\Omega(\mathbf{x}')}{V^{*}(\mathbf{x}')}\right\} \quad (33)$$

$$-\sum_{\alpha=1}^{\upsilon}\int_{\Omega(\mathbf{x})}\mathbf{\Phi}_{\eta}(\mathbf{x})\boldsymbol{\varphi}^{\alpha}\cdot\delta\mathbf{U}^{\eta,\alpha}\frac{d\Omega(\mathbf{x})}{V^{*}(\mathbf{x})}$$
$$\approx-\sum_{\alpha=1}^{\upsilon}\sum_{I_e=1}^{N_e}\sum_{g=1}^{8}\frac{J(I_e,g)}{V^{*}(I_e,g)}\mathbf{\Phi}_{\eta}(I_e,g)\boldsymbol{\varphi}^{\alpha}\cdot\delta\mathbf{U}^{I(\eta),\alpha} \quad (34)$$

where $J(I_e,g)$=Jacobian of the gth Gauss point of the I_eth element. Therefore, $\mathrm{N}(I_e,g)\equiv J(I_e,g)/V^{*}(I_e,g)$=number of unit cells that the gth Gauss point of the I_eth element represents and it is noticed that this number is constant in time. It is essentially the way to indicate that mass is conserved. Because Eq. (29) has to be valid for any arbitrary virtual displacement $\delta\mathbf{U}^{I,\beta}$ $(I=1,2,3,\ldots,N_p)$ $(\beta=1,2,\ldots,\upsilon)$, it leads to the following governing equations for nodal displacements

$$\sum_{I_e=1}^{N_e}\sum_{g=1}^{8}\mathbf{m}^{\beta}\mathbf{\Phi}_{\eta}(I_e,g)\mathbf{\Phi}_{\xi}(I_e,g)N(I_e,g)\ddot{\mathbf{U}}^{I(\xi),\beta}\tilde{\delta}[I-I(\eta)]$$
$$-\frac{1}{2}\sum_{\gamma=1}^{\upsilon}\sum_{I_e=1}^{N_e}\sum_{g=1}^{8}\tilde{\delta}[I-I(\eta)]\mathbf{\Phi}_{\eta}(I_e,g)N(I_e,g)\times\int_{\Omega(\mathbf{x}')}\mathbf{f}^{\beta\gamma}[\mathbf{u}^{\beta}(I_e,g),\mathbf{u}^{\gamma}(\mathbf{x}')]\frac{d\Omega(\mathbf{x}')}{V^{*}(\mathbf{x}')}$$
$$+\frac{1}{2}\sum_{\gamma=1}^{\upsilon}\sum_{I_e=1}^{N_e}\sum_{g=1}^{8}N(I_e,g)\int_{\Omega(\mathbf{x}')}\tilde{\delta}[I-J(\eta)]\mathbf{\Phi}_{\eta}(\mathbf{x}')\times\mathbf{f}^{\gamma\beta}[\mathbf{u}^{\gamma}(I_e,g),\mathbf{u}^{\beta}(\mathbf{x}')]\frac{d\Omega(\mathbf{x}')}{V^{*}(\mathbf{x}')}$$
$$-\sum_{I_e=1}^{N_e}\sum_{g=1}^{8}N(I_e,g)\mathbf{\Phi}_{\eta}(I_e,g)\boldsymbol{\varphi}^{\beta}\tilde{\delta}[I-I(\eta)]=0 \quad (35)$$

where $\tilde{\delta}$=Kronecker delta. It is emphasized that Eq. (35) is the FE formulation of this multiscale field theory. Note that the FE mesh with N_e element, the eight Gauss points per element, the shape functions $\mathbf{\Phi}_\eta(I_e,g)$, the integration over $\mathbf{\Omega}(\mathbf{x}')$, and the interatomic force $\mathbf{f}^{\beta\gamma}$ are involved in Eq. (35). It should also be emphasized that $\mathbf{f}^{\beta\gamma}$ is calculated exactly the same way as in the MD simulation.

It is noticed in Eq. (35) that the corresponding mass matrix $m^\beta \mathbf{\Phi}_\eta(I_e,g)\mathbf{\Phi}_\xi(I_e,g)\mathrm{N}(I_e,g)$ obtained from all Gauss points in all elements is symmetric but not diagonal. This is referred to as the distributed mass system. For the sake of dramatically reducing the computational effort, one would like to have a diagonal mass matrix, which is referred to as the lumped mass system. To do so, we let the eight Gauss points move toward their corresponding nodal points. In other words, let

$$\mathbf{\Phi}_\xi(I_e,g) \to \delta_{\xi g} \tag{36}$$

By doing so, not only do we end up with a lumped mass system, but we also convert the numerical implementation from Gauss integration to nodal integration if we choose to apply Eq. (36) to all other terms in Eq. (35).

It is seen that Eq. (35) is a set of $3\upsilon N_p$ second order ordinary differential equations, which can be readily solved by the central difference method. We have developed computer software, named Continuum Multiscale Modeling (CMM), which is based on the multiscale field theory and the above-mentioned finite-element formulation.

The idea of the finite-element analysis of this multiscale theory can be further elaborated as follows. From Eqs. (31)–(34), it is seen that we approximate the integral over the space $\mathbf{\Omega}(\mathbf{x})$ by the Gauss quadrature

$$\int_{\Omega(\mathbf{x})} \mathbf{A}(\mathbf{x}) \frac{d\Omega(\mathbf{x})}{V^*(\mathbf{x})} \approx \sum_{I_e=1}^{N_e} \sum_{g=1}^{8} \mathbf{A}(I_e,g) N(I_e,g) \tag{37}$$

where $\mathbf{A}$=integrand; $\{I_e,g\}$ stands for the position of the gth Gauss point in the I_eth element; and $\mathrm{N}(I_e,g)$=number of unit cells associated with that Gauss point. If one employs nodal integration in lieu of Gauss integration, then Eq. (37) can be rewritten as

$$\int_{\Omega(\mathbf{x})} \mathbf{A}(\mathbf{x}) \frac{d\Omega(\mathbf{x})}{V^*(\mathbf{x})} \approx \sum_{I_p=1}^{N_p} \mathbf{A}(I_p) N(I_p) \tag{38}$$

where $\mathbf{A}(I_p)$=integrand evaluated at the I_pth node; N_p=total number of FE nodes of the entire specimen; $\mathrm{N}(I_p)$=weight of the I_pth node, which is equal to the number of unit cells that the I_pth node represents. This idea can be further illustrated by Fig. 1, from which we see the specimen is divided into identical parallelepipeds—unit cells; each is made of a specified number of distinct atoms; we also see an irregular FE mesh (here a 2D mesh for the purpose of illustration), of which each node is a unit cell. To emphasize it graphically, the atoms in the nodes are shown in color; different colors represent different kinds of atoms. The shaded area around each node indicates a *cutoff* region within which all the atoms have atomistic interaction with the node. It is worthwhile to note that all unit cells, hence all the atoms, in the specimen are represented by the FE nodes and each node is weighted according to the number of unit cells that it represents [Eqs. (37) or (38)]; all the nodes have interactions with all the atoms within their *cutoff* regions [Eq. (35)]. If one would like to have the whole specimen covered by overlapping *cutoff* regions and also prefer to use large-size FE elements, one may use higher order Gauss integration of which the needed positions and weighting coefficients are given by Zienkiewicz and Taylor (1989).

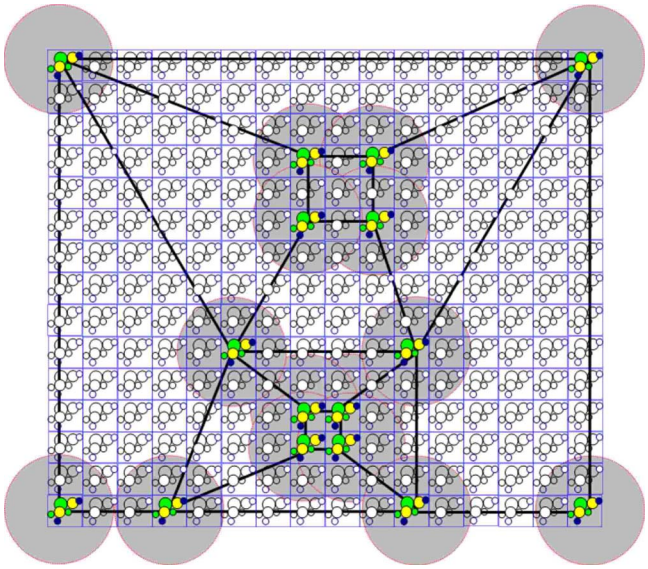

Fig. 1. Schematic diagram of crystal lattice, unit cells, finite-element mesh and nodes, and cutoff regions of a single crystal

Sample Problems

In this work, we present two sample problems: (1) wave propagation and (2) simple tension to demonstrate the advantage and applicability of this multiscale field theory. Atomic units are used throughout this paper, i.e.,

$$\text{mass} = \text{rest mass of electron: } m_e = 9.10938188 \times 10^{-31} \text{ kg};$$

$$\text{length} = \text{Bohr radius: } a_o = 0.529177249 \times 10^{-10} \text{ m};$$

$$\text{electron charge: } e = 1.602176462 \times 10^{-19} \text{ Coulomb};$$

$$\text{time: } \tau_o = m_e a_o^2/\hbar = 2.418884326555 \times 10^{-17} \text{ sec}; \quad \text{and}$$

$$\text{energy} = \text{Hartree: } E_h = \hbar^2/m_e a_o^2 = 4.3597482 \times 10^{-18} \text{ Joule}$$

In this work, we consider a single crystal *MgO*, which has a rocksalt-type crystal lattice. Each unit cell has eight atoms: four magnesium and four oxygen, located at [see. Fig. 2(c)]:

$$\text{Mg: } (0\ 0\ 0)\ \left(\frac{a}{2}\frac{a}{2}\ 0\right)\ \left(\frac{a}{2}\ 0\ \frac{a}{2}\right)\ \left(0\ \frac{a}{2}\frac{a}{2}\right)$$

$$\text{O: } \left(\frac{a}{2}\ 0\ 0\right)\ \left(0\ \frac{a}{2}\ 0\right)\ \left(0\ 0\ \frac{a}{2}\right)\ \left(\frac{a}{2}\frac{a}{2}\frac{a}{2}\right)$$

where a=7.93684912 Bohr is the lattice constant. The three base vectors are

$$\mathbf{v}_1 = (a\ 0\ 0) \quad \mathbf{v}_2 = (\ 0\ a\ 0) \quad \mathbf{v}_3 = (0\ 0\ a)$$

The Coulomb-Buckingham potential between two atoms, *atom* ξ and *atom* η, can be expressed as

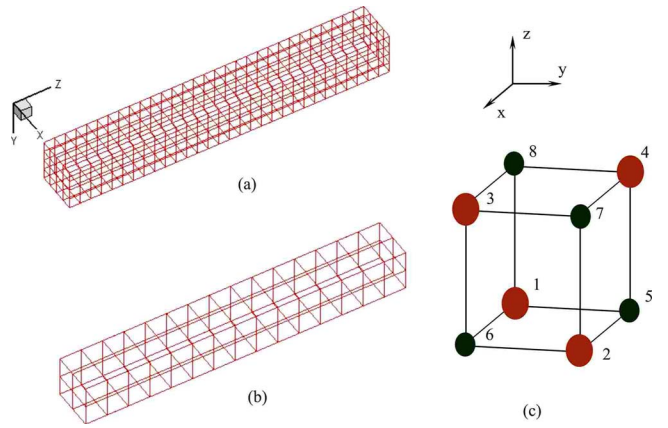

Fig. 2. Finite-element mesh of a specimen of magnesium oxide: (a) $4\times4\times30$ mesh; (b) $2\times2\times15$ mesh; and (c) crystal structure of MgO

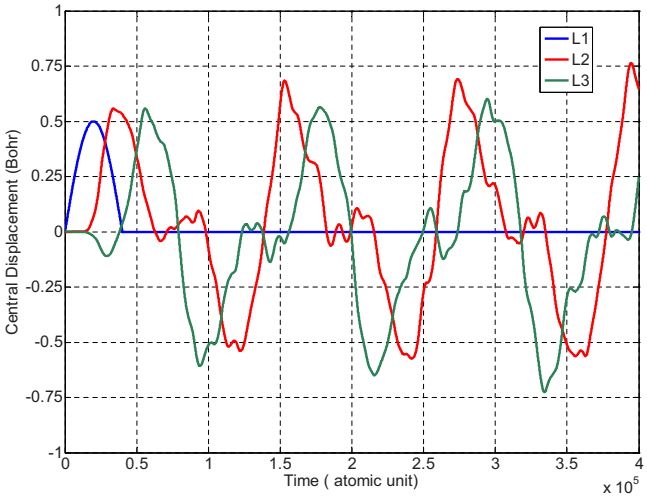

Fig. 3. Wave propagation in fine mesh FE model with acoustic input

$$V^{\xi\eta}=\frac{e^{\xi}e^{\eta}}{r^{\xi\eta}}+A^{\xi\eta}e^{-r^{\xi\eta}/B^{\xi\eta}}-C^{\xi\eta}/(r^{\xi\eta})^6 \tag{39}$$

where $A^{\xi\eta}$, $B^{\xi\eta}$, and $C^{\xi\eta}$ are material constants; $r^{\xi\eta}\equiv\|\mathbf{r}^{\xi\eta}\|\equiv\|\mathbf{r}^{\xi}-\mathbf{r}^{\eta}\|$. The interatomic forces can be obtained as

$$\mathbf{f}(\xi;\eta)=-\frac{\partial V^{\xi\eta}}{\partial\mathbf{r}^{\xi}}=-\frac{\partial V^{\xi\eta}}{\partial r^{\xi\eta}}\frac{\mathbf{r}^{\xi\eta}}{r^{\xi\eta}}=\left\{\frac{e^{\xi}e^{\eta}}{(r^{\xi\eta})^3}+\frac{A^{\xi\eta}}{B^{\xi\eta}r^{\xi\eta}}e^{-r^{\xi\eta}/B^{\xi\eta}}-6\frac{C^{\xi\eta}}{(r^{\xi\eta})^8}\right\}\mathbf{r}^{\xi\eta}$$

$$\mathbf{f}(\eta;\xi)=-\frac{\partial V^{\xi\eta}}{\partial\mathbf{r}^{\eta}}=-\mathbf{f}(\xi;\eta) \tag{40}$$

The material constants used in this work for MgO are

$$\text{mass(Mg)}=4.57636\times10^4 m_e \quad \text{mass(O)}=3.01251\times10^4 m_e$$

$$e^{\text{Mg}}=2e \quad e^{\text{O}}=-2e$$

$$A^{\text{Mg–Mg}}=C^{\text{Mg–Mg}}=0$$

$$A^{\text{Mg–O}}=47.2\ \text{Hartree} \quad B^{\text{Mg–O}}=0.56635\ \text{Bohr} \quad C^{\text{Mg–O}}=0$$

$$A^{\text{O–O}}=350.88\ \text{Hartree} \quad B^{\text{O–O}}=0.41415\ \text{Bohr}$$

$$C^{\text{O–O}}=53.554\ \text{Hartree Bohr}^6$$

In this work, the cutoff for the short-range Buckingham potential $A^{\xi\eta}e^{-r^{\xi\eta}/B^{\xi\eta}}-C^{\xi\eta}/(r^{\xi\eta})^6$ is set to be 22.6 Bohr; the Coulomb potential $(e^{\xi}e^{\eta})/(r^{\xi\eta})$ covers the whole specimen.

Wave Propagation

For this case, two finite-element models of a specimen are constructed as shown in Fig. 2. The first one has $4\times4\times30$ eight-node elements; each element is a cube with volume a^3 [Fig. 2(a)], the second one has $2\times2\times15$ eight-node elements; each element is a cube with volume $(2a)^3$ [Fig. 2(b)]. The specimen occupies the space: $0\leqslant x\leqslant4a$, $0\leqslant y\leqslant4a$, $0\leqslant z\leqslant30a$. The total number of unit cells of this specimen is $4\times4\times30=480$. In this analysis, we use 12,000 time steps, $\Delta t=40\ \tau_o$, and total time $T_f=480{,}000\ \tau_o=11.6$ pico secs. The system is assumed to be initially at rest after a period of relaxation time, and two types of boundary conditions are set as

1. Acoustic

$$u_z^{\alpha}(x,y,30a,t)=0 \tag{41}$$

$$u_z^{\alpha}(x,y,0,t)=\begin{cases}0.5\sin(\pi t/40{,}000) & \text{if } t\leqslant40{,}000\tau_o\\ 0 & \text{if } t>40{,}000\tau_o\end{cases} \tag{42}$$

where $\alpha=1,2,3,\ldots,8$.

2. Optic

$$u_z^{\alpha}(x,y,30a,t)=0 \tag{43}$$

$$u_z^{\alpha}(x,y,0,t)=\begin{cases}\pm0.3\sin(10\pi t/20{,}000) & \text{if } t\leqslant20{,}000\tau_o\\ 0 & \text{if } t>20{,}000\tau_o\end{cases} \tag{44}$$

where the "+" sign is for $\alpha=3, 4, 7, 8$ and the "−" sign for $\alpha=1,2,5,6$ [Fig. 2(c)].

The central displacement of a unit cell is defined as

$$\tilde{\mathbf{u}}\equiv\sum_{\alpha=1}^{8}\frac{m^{\alpha}}{M}\mathbf{u}^{\alpha} \tag{45}$$

and the relative displacement, relevant to this sample problem, of a unit cell is defined as

$$\hat{\mathbf{u}}\equiv\{\mathbf{u}^3+\mathbf{u}^4+\mathbf{u}^7+\mathbf{u}^8-\mathbf{u}^1-\mathbf{u}^2-\mathbf{u}^5-\mathbf{u}^6\}/\mathbf{8} \tag{46}$$

It is seen that $\tilde{\mathbf{u}}$ and $\hat{\mathbf{u}}$=measures of acoustic mode and optic mode, respectively.

For the first finite-element model in the case of acoustic input [Eqs. (41) and (42)], the central displacements $\tilde{u}_z$ at Point $L1$ $(2a,2a,0)$, Point $L2$ $(2a,2a,10a)$, and Point $L3$ $(2a,2a,20a)$ are plotted as functions of time in Fig. 3. The speed of longitudinal wave is obtained as 9,075 m/s, which is amazingly close to the experimental value around 9,100 m/s (Jackson and Niesler 1982). For the case of optic input [Eqs. (43) and (44)], the central displacements $\tilde{u}_z$ and the relative displacements $\hat{u}_z$ at Point $L1$ and Point $L3$ are plotted as functions of time in Figs. 4(a and b), respectively. It is noted that the ability to display an optic mode

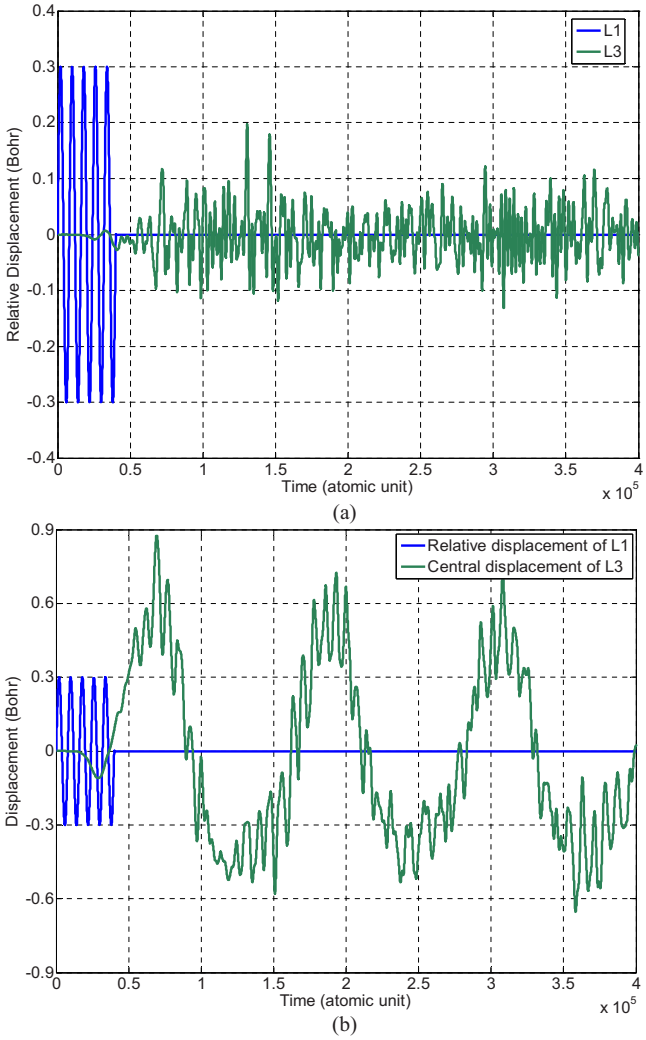

Fig. 4. Wave propagation in fine mesh FE model with optic input: (a) relative displacement versus time of L1 and L3; (b) central displacement versus time of L3

and the propagation of optic wave are the characteristics of our multiscale theory and its corresponding computer software.

For the second finite-element model, the corresponding results are shown in Figs. 5 and 6. It is noticed that the first finite-element model is actually a limiting case equivalent to a MD model. In other words, each node in the finite-element mesh is a unit cell, but there is nothing in the interior of any element. The speed of longitudinal wave of the second FE model is obtained as $9,027$ m/s. This means the change of element size from a^3 to $8a^3$ does not change the longitudinal wave speed practically. However, the magnitude of the relative displacement (optic mode) of the second FE model is about half of that from the first FE model. This may be explained as follows. In FE analysis, an assemblage with larger elements gives a smaller cutoff frequency. Therefore, the second FE model has a smaller cutoff frequency than the first one. For a wave with a frequency greater than the cutoff frequency of a FE model, the interface between elements appears as an almost rigid boundary that reduces the magnitude of the passing through a wave (Holmes and Belytschko 1976; Xiao and Belytschko 2004).

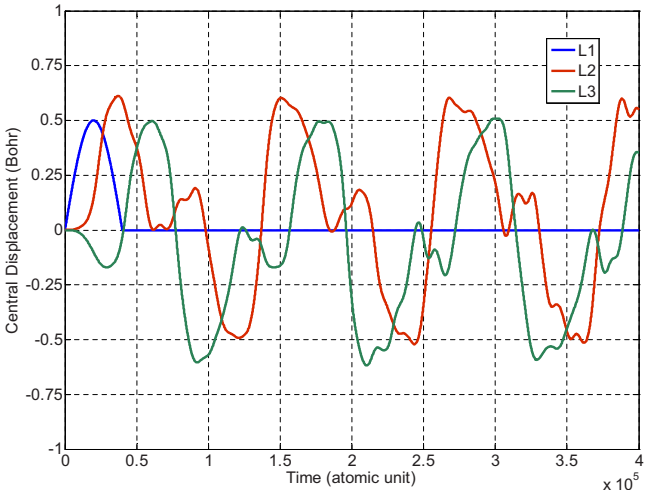

Fig. 5. Wave propagation in coarse mesh FE model with acoustic input

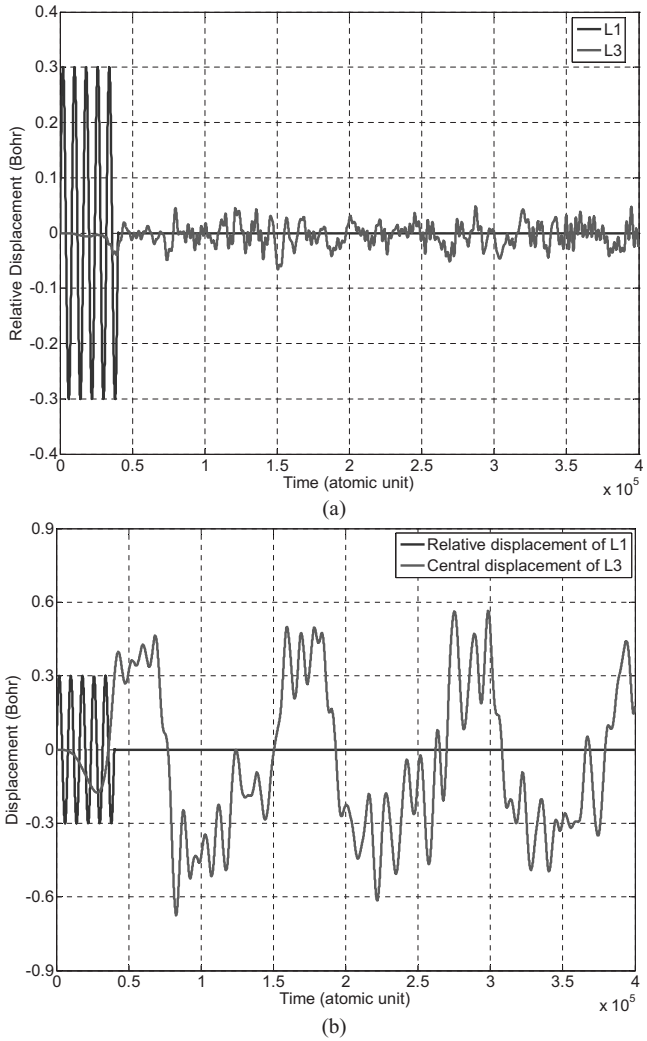

Fig. 6. Wave propagation in coarse mesh FE model with optic input: (a) relative displacement versus time of L1 and L3; (b) central displacemen versus time of L3

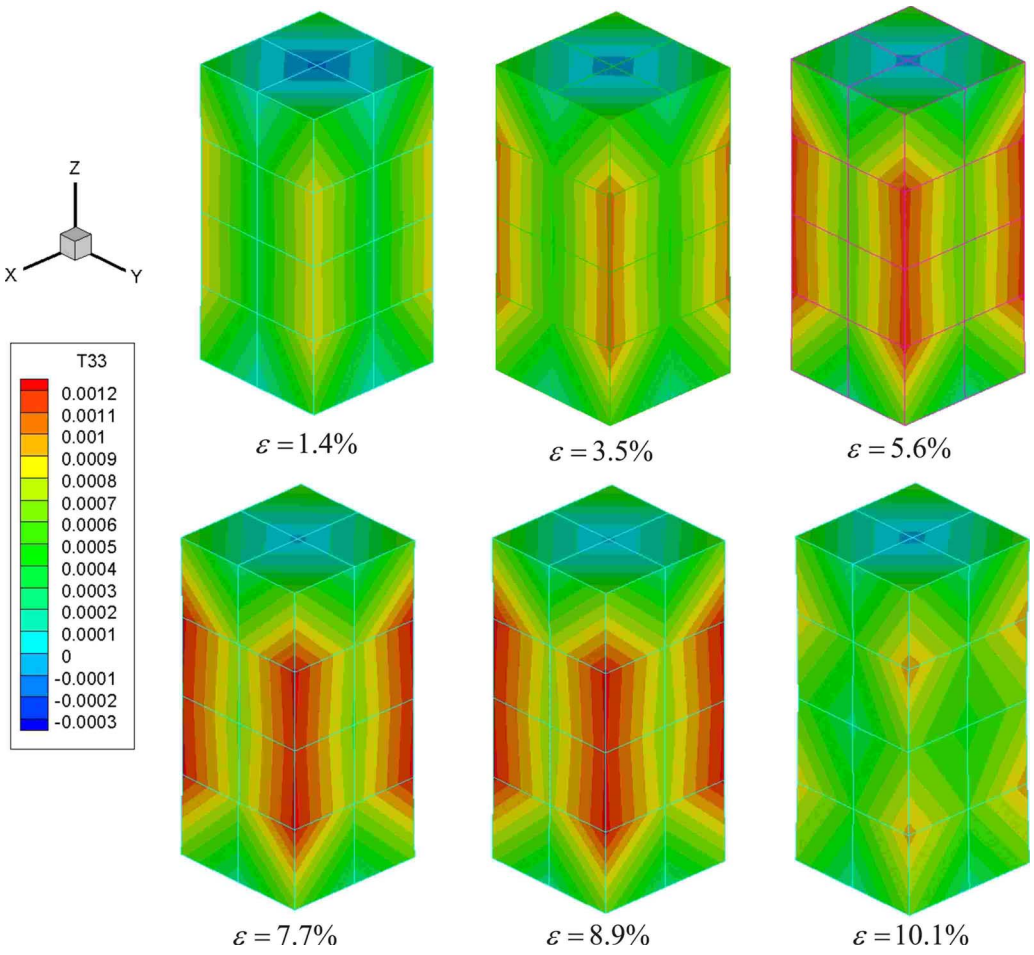

Fig. 7. Stress distributions (σ_{zz}) at different strains (ε_{zz}) in specimen under simple tension

Simple Tension

For this case, the finite-element model of the specimen has $2\times2\times4$ eight-node elements and 45 nodes; each element is a cube with volume (23.810547 Bohr$=3a)^3$; the total number of unit cells is 432. The specimen occupies a region $0\leqslant x\leqslant 6a$, $0\leqslant y\leqslant 6a$, $0\leqslant z\leqslant 12a\equiv H$. In this analysis, the magnitude of the time step is set to be $\Delta t=40\ \tau_o$ and the system is assumed to be initially at rest after a period of relaxation time with the following boundary conditions:

$$u_z^{\alpha}(x,y,0,t) = -0.5\varepsilon Ht/t_r \tag{47}$$

$$u_z^{\alpha}(x,y,H,t) = 0.5\varepsilon Ht/t_r \tag{48}$$

The rise time and the elongation are chosen to be $t_r=5.8\times10^6\ \tau_o$ and $\varepsilon=0.12$, respectively. The time history of the distribution of stress σ_{zz} on the deformed shape is plotted in Fig. 7. The stress-strain relation σ_{zz} versus ε_{zz} is shown in Fig. 8. The simulation results show that the Young's modulus, the von Mises yield strength, and the Poisson ratio are obtained as

$$E = 7.55\times10^{-3}\ \text{Hartree/Bohr}^3 = 218\ \text{GPa}$$

$$\sigma_Y = 3.71\times10^{-4}\ \text{Hartree/Bohr}^3 = 10.9\ \text{GPa}$$

$$\mu = 0.22$$

The experimental values for Young's modulus and Poisson's ratio are reported to be in the ranges of 192.9–319.1 GPa and 0.157–0.189, respectively in the NISTIR report (Munro 2002). The value of von Mises yield strength from MD simulation is obtained as 11.2 GPa (Xiong et al. 2006). It is seen that, although our Poisson's ratio is 16% higher than the reported experimental data, the Young's modulus is well within the range of reported

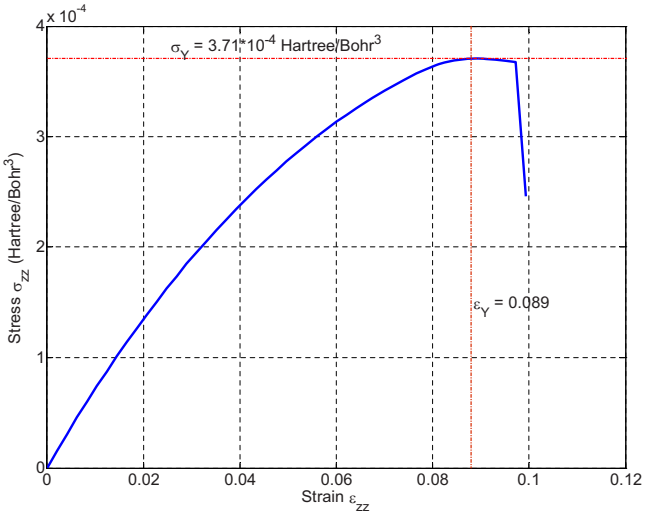

Fig. 8. Stress-strain relation ($\sigma_{zz}-\varepsilon_{zz}$) of MgO under simple tension

experimental data. The value of the von Mises yield strength from the finite-element analysis of this multiscale theory is amazingly close to the MD simulation value.

Summary and Discussion

We have briefly introduced a multiscale field theory and the governing equations for an atomistic multielement system (Chen 2006; Chen and Lee 2005, 2006; Chen et al. 2006a,b). Although the multiscale theory is on the same physical foundation as the MD simulation, we constructed a continuum theory, which is the field representation of atomistic *N-body* dynamics. Here, the term "multielement system" refers to a material system, which is made of more than one kind of chemical element. Therefore, in our multiscale theory, each point in the field represents one unit cell, which is made of several different and distinct atoms. For example, there are five atoms {one bismuth, one scadium, three oxygen} in a unit cell of $BiScO_3$ and eight atoms {four magnesium, four oxygen} in a unit cell of MgO.

In this work, from the balance law of linear momentum, we formulate the governing equations for an atomistic multielement system with given temperature and then we proceed rigorously to formulate the dynamic FE equations. For each FE node, there are 3υ displacements and υ=number of atoms in a unit cell, for example, $\upsilon=5$ for $BiScO_3$ and $\upsilon=8$ for MgO. It is noticed that $\upsilon=1$ only in classical continuum theory. Further, even at the continuum level, in the FE analysis, the nodal forces are calculated through the use of interatomic potentials between different pairs of atoms. It is worthwhile to note, in this work, we use pair potentials. However, the numerical framework does allow one to generalize to the level of many-body potentials, such as Tersoff potential. Therefore, our FE analysis is dynamic, nonlinear, and nonlocal. More importantly, in our computer software, the finest FE mesh one can use is equivalent to the crystal lattice; in other words, the smallest FE element size is equal to the lattice constant. Because one may use an irregular FE mesh with small-sized elements in critical regions and large-sized elements in far field, we do not need "bridging," "handshaking," or "transition" regions if we choose not to have.

From a *lattice dynamics* viewpoint, for crystals that have more than one atom in the unit cell, elastic distortions give rise to wave propagation of two types, acoustic and optic. In acoustic type, all atoms in the unit cell move essentially in the same phase, resulting in the deformation of a lattice. In optic type, the movement of all atoms gives rise to internal deformation and leaves the lattice unchanged. Therefore, to demonstrate this theory's capability to present these two modes, we give the definitions of central displacement and relative displacement for acoustic mode and optic mode, respectively; and then in the sample problem we show the propagation of optic wave. What has been discussed above is essentially the characteristic difference between our multiscale theory and the classical continuum theories. The continuum region in almost all the other multiscale theories that we mentioned in the Introduction is practically described by classical continuum theory.

The computer software (CMM) accompanying our multiscale theory gives numerical results that are in good agreement with either experimental value or result from MD simulation (see the section of Sample Problems):

1. Longitudinal wave speed:

$$v_L = 9{,}075 \text{ m/s (CMM, first FE model)}$$

$$v_L = 9{,}027 \text{ m/s (CMM, second FE model)}$$

$$v_L = 9{,}100 \text{ m/s (experimental)}$$

2. Young's modulus

$$E = 218 \text{ GPa (CMM)}$$

$$E \in [192.9, 319.1] \text{ GPA (experimental)}$$

3. von Mises yield strength

$$\sigma_Y = 10.9 \text{ GPa (CMM)}$$

$$\sigma_Y = 11.2 \text{ GPa (MD)}$$

In a future study, we may extend this approach to a material system, which consists of single crystal, modeled by this multiscale continuum field theory, and amorphous material, modeled by a large number of different kinds of discrete atoms as in the MD simulation. This can be readily done if one incorporates the atomistic interaction between atoms in the continuum domain and atoms in the discrete region. Of course, it is based on the availability of interatomic potentials. In fact, it can be further extended to the study of a material system, which consists of amorphous materials and polycrystals, considered as a collection of continua; each is modeled as a different and distinct single crystal. It is our reasonable expectation that (1) as long as there is an availability of interatomic potentials, this multiscale field theory works equally well for metallic materials and nonmetallic materials such as dielectric, piezoelectric, and ferroelectric materials, and semiconductor materials, etc., and (2) it works as an alternative to MD for statistical and finite-temperature properties of materials, but with significant advantages over MD in studying simultaneously large length and time scale properties.

Acknowledgments

The writers acknowledge the support by the National Science Foundation under Award No. CMMI-0646674.

References

Abraham, F. F., Broughton, J. Q., Bernstein, N., and Kaxiras, E. (1998). "Spanning the continuum to quantum length scales in a dynamic simulation of brittle fracture." *Europhys. Lett.*, 44(6), 783–787.

Adelman, S. A., and Doll, J. D. (1976). "Generalized Langevin equation approach for atom/solid surface scattering: General formulation for classical scattering off harmonic solids." *J. Chem. Phys.*, 64, 2375–2388.

Belytsckko, T., and Xiao, S. P. (2003). "Coupling methods for continuum model with molecular model." *Int. J. Multiscale Comp. Eng.*, 1, 115–126.

Broughton, J. Q., Abraham, F. F., Bernstein, N., and Kaxiras, E. (1999). "Concurrent coupling of length scales: Methodology and applications." *Phys. Rev. B*, 60, 2391–2402.

Cai, W., de Koning, M., Bulatov, V. V., and Yip, S. (2000). "Minimizing boundary reflections in coupled-domain simulations." *Phys. Rev. Lett.*, 85(15), 3213–3216.

Chen, Y. (2006). "Local stress and heat flux in atomistic systems involving three-body forces." *J. Chem. Phys.*, 124, 054113.

Chen, Y., and Lee, J. D. (2005). "Atomistic formulation of a multiscale theory for nano/micro physics." *Philos. Mag.*, 85, 4095–4126.

Chen, Y., and Lee, J. D. (2006). "Conservation laws at nano/micro scales." *J. Mech. Mater. Struct.*, 1, 681–704.

Chen, Y., Lee, J. D., Lei, Y., and Xiong, L. (2006a). "A multiscale field theory: Nano/micro materials." *Multiscaling in molecular and continuum mechanics*, G. C. Sih, ed., Springer, New York, 23–65.

Chen, Y., Lee, J. D., and Xiong, L. (2006b). "Stresses and strains at nano/micro scales." *J. Mech. Mater. Struct.*, 1, 705–723.

Cheung, K. S., and Yip, S. (1991). "Atomic-level stress in an inhomogeneous system." *J. Appl. Phys.*, 70(10), 5688–5690.

Curtin, W. A., and Miller, R. E. (2003). "Atomistic/continuum coupling in computational materials science." *Modell. Simul. Mater. Sci. Eng.*, 11, R33–R68.

Doll, J. R., and Dion, D. R. (1976). "Generalized Langevin equation approach for atom/solid surface scattering: Numerical techniques for Gaussian generalized Langevin dynamics." *J. Chem. Phys.*, 65, 3762–3766.

Dove, M. (1993). *Introduction to lattice dynamics*, Cambridge University Press, Cambridge, U.K.

Dupuy, L. M., Tadmor, E. B., Miller, R. E., and Phillips, R. (2005). "Finite temperature quasicontinuum: Molecular dynamics without all the atoms." *Phys. Rev. Lett.*, 95, 060202.

E, W., Engquist, B., Li, X., Ren, W., and Vanden-Eijnden, E. (2007). "The heterogeneous multiscale method: A review." *Comm. Comp. Phys.*, 2(3), 367–450.

E, W., and Huang, Z. (2001). "Matching conditions in atomistic-continuum modeling of materials." *Phys. Rev. Lett.*, 87, 135501.

E, W., and Huang, Z. (2002). "A dynamic atomistic-continuum method for the simulation of crystalline materials." *J. Comput. Phys.*, 182, 234–261.

Haile, J. M. (1992). *Molecular dynamics simulation*, Wiley, New York.

Hardy, R. J. (1982). "Formulas for determining local properties in molecular-dynamics simulations: Shock waves." *J. Chem. Phys.*, 76(1), 622–628.

Holmes, N., and Belytschko, T. (1976). "Postprocessing of finite-element transient response calculations by digital filters." *Comput. Struct.*, 6, 211–216.

Irvine, J. H., and Kirkwood, J. G. (1950). "The statistical theory of transport processes. IV: The equations of hydrodynamics." *J. Chem. Phys.*, 18, 817–829.

Jackson, I., and Niesler, H. (1982). "The elasticity of periclase to 3 GPa and some geophysical implications." *Advances in earth and planetary sciences 12, high-pressure research in geophysics*." S. Akimoto and M. H. Manghnani, eds., Centre for Academic Publications, Boston, 93–113.

Karpov, E. G., Wagner, G. J., and Liu, W. K. (2005). "A Green's function approach to deriving non-reflecting boundary conditions in molecular dynamics simulations." *Int. J. Numer. Methods Eng.*, 62(9), 1250–1262.

Knap, J., and Ortiz, M. (2001). "An analysis of the quasicontinuum method." *J. Mech. Phys. Solids*, 49, 1899–1923.

Li, X., and E, W. (2005). "Multiscale modeling of dynamics of solids at finite temperature." *J. Mech. Phys. Solids*, 53, 1650–1685.

Liu, B., Huang, Y., Jiang, H., Qu, S., and Hwang, K. C. (2004). "The atomic-scale finite-element method." *Comput. Methods Appl. Mech. Eng.*, 193, 1849–1864.

Munro, R. G. (2002). "Elastic moduli data for polycrystalline ceramics." *NISTIR 6853*, National Institute of Standards and Technology, Gaithersburg, Md.

Rudd, R. E. (2001). "Concurrent multiscale modeling of embedded nanomechanics." *Mater. Res. Soc. Symp. Proc.*, 677, AA1.6.1–AA1.6.12.

Rudd, R. E., and Broughton, J. Q. (1998). "Coarse-grained molecular dynamics and the atomic limit of finite element." *Phys. Rev. B*, 58, R5893–R5896.

Rudd, R. E., and Broughton, J. Q. (2000). "Concurrent coupling of length scales in solid state systems." *Phys. Status Solidi B*, 217, 251–291

Shenoy, V. B., Miller, R., Tadmor, E. B., Rodney, D., Phillips, R., and Ortiz, M. (1998). "An adaptive methodology for atomic scale mechanics: The quasicontinuum method." *J. Mech. Phys. Solids*, 47, 611–642.

Tadmor, E. B., Ortiz, M., and Phillips, R. (1996). "Quasicontinuum analysis of defects in solids." *Philos. Mag. A*, 73, 1529–1563.

To, A. C., and Li, S. (2005). "Perfectly matched multiscale simulations." *Phys. Rev. B*, 72(3), 035414.

Wagner, G. J., and Liu, W. K. (2003). "Coupling of atomistic and continuum simulations using a bridging scale decomposition." *J. Comput. Phys.*, 190, 249–274.

Xiao, S. P., and Belytsckko, T. (2004). "A bridging domain method for coupling continua with molecular dynamics." *Comput. Methods Appl. Mech. Eng.*, 193, 1645–1669.

Xiong, L., Chen, Y., and Lee, J. D. (2006). "Atomistic measure of the strength of MgO nanorods." *Theor. Appl. Fract. Mech.*, 46, 202–208.

Xiong, L., Chen, Y., and Lee, J. D. (2007). "Atomistic simulation of mechanical properties of diamond and silicon by a field theory." *Modell. Simul. Mater. Sci. Eng.*, 15, 535–551.

Zienkiewicz, O. C., and Taylor, R. L. (1989). *The finite-element method, Vol.1, basic formulation and linear problems*, McGraw-Hill, London.